Catalysis Letters Vol. 109, Nos. 3–4, July 2006 (© 2006)
DOI: 10.1007/s10562-006-0067-1

Non-metal catalysts for dioxygen reduction in an acidic electrolyte

Paul H. Matter and Umit S. Ozkan*

Department of Chemical Engineering, The Ohio State University, 140 W. 19th Ave., Columbus, OH 43210, USA

Received 12 January 2006; accepted 20 March 2006

Active non-metal catalysts for the Oxygen Reduction Reaction (ORR) were prepared by decomposition of acetonitrile vapor at 900°C over a pure alumina support, and supports containing 2 wt% Fe or 2 wt% Ni on alumina. The exposed alumina and metal in the samples were subsequently washed away with HF acid to purify the solid carbon material. The sample prepared with iron was the most active sample for the ORR, with only 100 mV greater overpotential than a commercial 20 wt% Pt / Vulcan Carbon catalyst. However, nitrogen-containing carbon deposited on pure alumina (which contained less than 1 ppm metal contamination) was also quite active, demonstrating that platinum or iron is not required for ORR activity. Characterization by XPS and TEM revealed that the more active samples had nanostructured carbon with more edge plane exposure than the less active tube structures formed from the nickel sample.

KEY WORDS: PEM fuel cells; oxygen reduction; nitrogen-containing carbon; carbon nanostructure.

1. Introduction

Reducing the use of platinum in PEM fuel cell systems has been identified as a major requirement for the wide-scale commercialization of these low temperature energy conversion devices, especially for use in automobiles. Particularly, developing alternative catalysts to platinum for the Oxygen Reduction Reaction (ORR) in the cathode of the fuel cell is of high priority because the slow kinetics of this reaction causes significant efficiency losses in the cell. Alternative catalysts based on pyrolyzed iron, carbon, and nitrogen compounds have been investigated recently, and activity of these catalysts is found comparable to commercial platinum catalysts [1–12].Various sites have been attributed to the improved activity of these mostly carbon materials, with sites ranging from iron ions stabilized by nitrogen groups on the carbon surface [3] to non-metallic active sites [13–18]. Although iron-containing catalysts are generally more active than samples without iron, some researchers have hypothesized that iron may not be part of the active site, but may simply act as a catalyst for the formation of the active site during the heat treatment [5, 12, 15–17]. Evidence for such a hypothesis includes the presence of unique nanostructures in pyrolyzed Fe / N / C samples [12, 16, 17], and the fact that activity can improve after treatments with acid or Cl_2, which removes exposed iron [5]. Additionally, carbon samples that contained as low as 70 ppm iron contamination showed good activity after a high temperature treatment with a nitrogen source [10].

*To whom correspondence should be addressed.
E-mail: ozkan.1@osu.edu

In recent work, our group demonstrated that iron can act as a catalyst for the formation of carbon fibers during the pyrolysis of acetonitrile over Vulcan Carbon doped with 2% Fe 12]. These fibers had a nanostructure that resulted in a high percentage of carbon edge plane exposure. Consequently, these materials were more active for the ORR than iron-free samples (Ni-doped or undoped), which did not lead to nanostructured carbon, although all the nitrogen-containing carbon samples had improved activity compared to untreated carbon. This has led us to hypothesize that the active site for the ORR is located on the edge plane of nitrogen-containing carbon, and the iron-containing samples are more active because iron is acting as a catalyst for the formation of carbon nano-structures with a higher exposure of edge planes. Two possibilities for the improved activity include pyridinic nitrogen sites, which could potentially interact with O_2, and/or the improved electron donating properties of nitrogen-containing carbon that could be propagated to O_2 adsorbed on edge planes. An active site has also been proposed, by other researchers, consisting of iron stabilized by pyridinic nitrogen groups on the carbon edge plane [3]. Such a site can not be ruled out since the carbon support inherently contains metal contamination. In an effort to answer this question, in the current study we examine nitrogen-containing carbon catalysts prepared by decomposition of acetonitrile over an alumina support that contains less than 1 ppm metal contamination. Such experiments could definitively show if iron is part of the active site for the ORR, or merely acting as a catalyst for the formation of favorable carbon structures. While alumina is electrically not conductive, the nitrogen-containing carbon deposited on the support can still be tested for ORR

activity in a Rotating Ring-Disk Electrode (RRDE) half cell set-up. Moreover, the alumina can be removed from the carbon by washing with a strong acid. In some cases of this study, the alumina support was doped with iron or nickel to catalyze the formation of various nanostructures during the pyrolysis of acetonitrile to further examine the effect of structure on ORR activity.

Supported metal particles, particularly Fe, Co, and Ni are known to catalyze the formation of various nanostructures during treatments above 550°C in carbon rich non-oxygenating atmospheres. Rodriquez and Baker have demonstrated several different structures that can form catalytically during the decomposition of hydrocarbons in the presence of various metal / support systems [19–21]. Park and Keane have also extensively examined the growth of nanostructures from various supported metal particles [22]. Therefore, in this work we further investigate the role of alumina-supported Fe and Ni in the formation of specific nitrogen-containing carbon nanostructures from acetonitrile, and the relation to ORR activity. Characterization of the materials was conducted with Transmission Electron Microscopy (TEM) and X-ray Photo-electron Spectroscopy (XPS). Particularly, XPS and TEM characterization were used to verify the role of the support in forming specific nanostructures. Characterization results are correlated to oxygen reduction activity and selectivity determined from RRDE half cell experiments.

2. Experimental methods

2.1. Catalyst preparation

In-house prepared alumina was used as a support for the high temperature pyrolysis of acetonitrile to produce active catalysts. The high purity alumina was prepared by a sol-gel technique, in which aluminum tri-sec-butoxide (Aldrich, 97%, <1 ppm metals contamination) was mixed with ethanol (HPLC grade) in a 1:2 mass ratio. After stirring vigorously for 5 minutes, demineralized water was added using a syringe pump at 0.5 mL/min while stirring to obtain the final water to ATB mole ratio of 4:1. The pH of the gel was then adjusted to 5 using several drops of concentrated HNO_3. The sample was dried overnight at room temperature. The resulting solid was crushed then calcined at 800°C in air for 2 hours. All glassware that came in contact with the alumina was cleaned beforehand with nitric acid (Fisher, 0.04 ppm Fe) and double distilled water to limit metal contamination. In the cases where the support was doped with a metal prior to acetonitrile deposition, the desired amount of metal acetate salt was dissolved in 100 mL of double distilled H_2O, then the support was added to the solution while stirring vigorously. The sample was then stirred an additional 30 minutes and sonicated 20 minutes before drying overnight at 100°C.

Acetonitrile decomposition, or pyrolysis, was carried out by first adding 2.0 g of support to a quartz calcination boat, and sealing it inside a quartz tube furnace. The temperature was then ramped at 10°C/min up to the treatment temperature under the carrier gas (N_2 unless noted otherwise) flowing at 150 sccm. Once the furnace reached the desired treatment temperature, the room temperature carrier gas was saturated with acetonitrile (P_{vap} = 72.8 mm Hg at 25°C) using a bubbler before being sent to the furnace. After 2 hours of treatment the samples were cooled to room temperature under the carrier gas.

In the next step, samples were washed with HF acid (aqueous 49% by weight) to remove any exposed metal and alumina. Approximately 0.5 g of sample was placed in a Nalgene beaker and 10 mL of concentrated HF was added slowly. The mixture was stirred and allowed to sit for several hours. Then, 500 mL of demineralized H_2O was added slowly, and the undissolved carbon sample was washed by suction filtration using an additional 1.5 L of double distilled H_2O.

2.2. XPS

X-ray photoelectron spectroscopy analysis was performed using a Kratos Ultra Axis Spectrometer on samples to determine surface composition of the elements present, and to gain insight about the nature of functional groups on the surface. For each sample a survey was performed from 1200 to 0 eV using a Mg anode at 14 kV, and a 10 mA current. Next, 5 sweeps were carried out for each element concurrently, with the Al 2p, C 1s, N 1s, and O 1s region always being scanned.

2.3. TEM

Transmission electron microscopy was performed with a Phillips CM300 Ultra-Twin FEG TEM and also a Phillips Tecnai TF20. Samples were supported by lacey-formvar carbon, which was supported by a 200 mesh copper grid. The carbon samples were dispersed with excess ethanol before being deposited of the grid.

2.4. Activity testing

The activity of all samples for the ORR was gauged with Cyclic Voltammetry (CV) experiments using a PAR BiStat with a model 636 RRDE set-up. First, a catalyst ink was prepared using one part (by mass) of catalyst and ten parts of 0.5 wt% Nafion in aliphatic alcohols. After sonicating the ink, approximately 10 μL was dispensed on the glassy carbon disk so as to completely cover the glassy carbon current collector with a thin film of catalyst, but not cover the platinum ring or Teflon casing of the RRDE. The inks were also used for conductivity measurements, described elsewhere [12]. For the testing, a 0.5 M solution of H_2SO_4 was used as the

electrolyte. The solution was purged with pure O_2 before performing an initial test sweep from 1.2 to 0 V (vs. NHE) at 10 mV/s to remove gaseous O_2 from the catalyst pores and allow the pores to fill with solution. Next, the solution was sparged with argon for 30 minutes to remove O_2 from the electrolyte. Then, five consecutive CV's were run on the disk from 1.2 to 0.0 to 1.2 V (vs. NHE) at 50 mV/s to confirm that there is no oxygen remaining, and to obtain a steady current by cleaning reducible and oxidizable contaminants off the electrode. Next, a baseline for the disk was obtained by sweeping from 1.2 to 0.0 to 1.2 V (vs. NHE) at 10 mV/s in the argon sparged solution at a 100 rpm rotation rate. Simultaneously, a background for the ring was obtained while holding the voltage of the Pt ring at 1.2 V vs. NHE. Finally, the solution was saturated with O_2 until consecutive CV's for the disk match (1.2 to 0.0 to 1.2 V at 50 mV/s), and slow CV's (10 mV/s) were then taken at rotations of 0 rpm, 100 rpm, and 1000 rpm. The peak in reduction current on the disk during the initial sweep without rotation is reported as a measurement of ORR activity. During the CV at 100 rpm, the ring potential was held at 1.2 V vs. NHE, and its current was monitored to detect any H_2O_2 production originating from the sample (on the disk). A higher amount of current in the ring indicates higher selectivity of the sample to peroxide, an undesirable byproduct. The RRDE manufacturer reports the collection efficiency of the ring to be 20% under laminar flow conditions. The reported ring currents are multiplied by 5 to correct for this efficiency.

3. Results and discussion

3.1. Catalyst preparation and physical characterization

The growth of carbon nano-fibers has been extensively studied using Fe, Co, and Ni-based catalysts in a carbon rich atmosphere [20, 23, 24]. Depending on the catalyst used and the atmosphere, fiber growth usually initiates near a temperature of 600°C, the temperature at which carbon can adsorb on the metal surface, diffuse through the metal particle, and deposit out the opposing side of the particle in the form of elemental carbon [20, 23]. Nitrogen-containing carbon fibers can require higher temperatures for significant growth. Fibers have been grown from acetonitrile and other vapors using Ni and Co based catalysts [25, 26], and as mentioned previously, fiber formation has been observed for Fe-doped Vulcan Carbon treated with acetonitrile at elevated temperatures [5, 12]. Using carbon as a support is more practical for use in an actual fuel cell; however, sol-gel alumina used in this study was better suited to address questions that cannot be studied using a carbon support like Vulcan Carbon for several reasons. First, alumina can be made in the lab with well-defined characteristics and high purity, unlike commercial carbons that will contribute Fe contamination and a large distribution of ill-defined and potentially reactive surface carbon-oxide species. Second, the alumina itself is not conductive and has no activity for the ORR, thus its presence cannot likely contribute to activity. Third, it is possible to selectively remove the alumina after the pyrolysis by treatment with a strong acid (HF) leaving behind only the nitrogen-containing carbon that formed during the acetonitrile decomposition.

When using Vulcan Carbon as a support for CH_3CN decomposition, the most active catalysts resulted from treatments at 900°C for 2 h. Therefore, for comparison purposes, samples were prepared using the three different supports (pure alumina, 2% Fe on alumina, and 2 Ni on alumina) under the same conditions. The properties of the catalysts prepared are shown in Table 1. The "weight gain" column indicates the percentage of weight increase of the sample during the acetonitrile decomposition from the deposition of nitrogen-containing carbon on the surface. The nitrogen content was determined from XPS and will be discussed in more detail in the following section. The ORR activity was measured in half cell testing, and the voltage at which the reduction current peaks is reported as a measure of activity. The current of the more active samples peaks at a higher voltage. This technique is commonly used by ORR catalyst researchers for gauging activity. As a reference, a 20 wt% Pt / VC commercial catalyst (Electrochem, EC20PTC), had an ORR peak potential of 750 mV vs. NHE in our experiments, and pure Vulcan carbon did not reduce oxygen until around 30 mV.

The results presented in Table 1 are significant for two main reasons. First, with respect to ORR activity, the sample that contained no metal had rather high activity for the ORR, although the Fe sample still had

Table 1
Properties of alumina-based supports after treatment in acetonitrile

Sample	% weight increase	BET S.A. (m^2/g)	N composition from XPS	ORR current peak (mv)
calcined sol-gel AI_2O_3	–	270	0.0%	–
AI_2O_3/CH_3CN-2 hours	23%	270	7.1%	490
AI_2O_3/CH_3CN-12 hours	99%	70	6.2	380
$Fe/AI_2O_3/CH_3CN$-2 hours	29%	70	5.1%	630
$Ni/AI_2O_3/CH_3CN$-2 hours	24%	90	4.8%	275

the highest activity. This shows that the mere presence of Fe cannot be pinpointed as the source of improved activity compared to pure carbon since the pure alumina sample (less than 1 ppm metal contamination) performed well. Second, the results presented in Table 1 make it apparent that the activity differences cannot be explained simply by physical property differences, especially when one considers samples such as alumina treated 12 h, and Fe/Al_2O_3 and Ni/Al_2O_3 treated 2 h that have nearly the same surface area and similar nitrogen contents, but a range of activities.

Since these samples primarily consist of alumina, which is a poor conductor and is not likely to be contributing any favorable electrochemical effects, experiments were carried out where the alumina was removed from the samples by treating them with hydrofluoric acid. This procedure also makes characterization of the active material easier since it essentially purifies the carbon that formed during the acetonitrile treatment. The properties of the nitrogen-containing carbon samples that formed from 2 h of acetonitrile decomposition and were subsequently washed with HF acid are shown in Table 2. The first column of data indicates that all of the samples lost a significant amount of mass during the acid wash. XPS analysis of the samples following the HF wash (data not shown) did not show any form of aluminum in any of the three samples. Fluorine was not detected either, with the only elements detected being carbon, nitrogen, and oxygen. In contrast, the unwashed samples contained a mixture of aluminum oxide and nitride that comprised roughly 10% of the surface of the surface composition of the samples, as determined from XPS (see Figure 1). The spectra resembled the spectra of AlN that has been exposed to oxygen [27]. The HF washed Fe- and Ni- derived samples contained metal particles encapsulated by carbon that were undetectable by XPS, but were evident in TEM and were physically visible after oxidation of the carbon. However, oxidation of the HF washed carbon formed on the pure alumina sample did not leave behind any visible residue.

The properties of the samples changed after removal of alumina from the samples, as the results in Table 2 indicate. After the acid wash all the samples underwent a large increase in surface area, and showed a modest

Table 2
Properties after HF wash of nitrogen-containing carbon samples prepared from acetonitrile decomposition at 900°C

Initial platform	%weight lost	BET S.A. (m^2/g)	N composition from XPS	ORR current peak(mv)	Conductivity (S/m)
AI_2O_3	−85%	810	5.2%	540	2.1
$2\%Fe/AI_2O_3$	−73%	570	5.1%	650	12
$2\%Ni/AI_2O_3$	−66%	500	4.1%	330	16

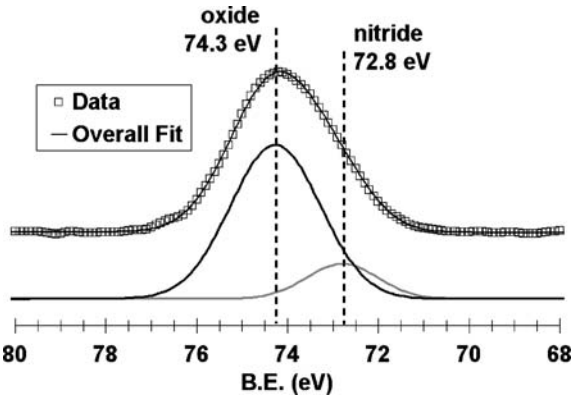

Figure 1. XPS analysis of Al 2p region for sol-gel alumina after treatment at 900°C for 2 hours in acetonitrile atmosphere.

improvement in ORR activity. The nitrogen content of the surface decreased in the samples from the removal of aluminum nitride. The increase in activity could be attributed to the removal of inactive alumina (which previously occupied roughly 10% of the surface). The large increase in surface area could also have a small effect on the peak location by increasing the reduction current at kinetic limited potentials. The conductivities of the dried catalyst inks were slightly less than Vulcan Carbon XC-72 (measured to be 71 S/m using the same procedure).

The most striking result from these experiments is again the large difference in activity between the samples, despite the similarities of the other properties. This activity difference cannot be attributed to the presence of Fe, since not only did the pure Al_2O_3 sample perform well, but also, all of these samples were treated with such a strong acid that any exposed metal would have been dissolved and washed away. More details of the XPS analysis reveal crucial differences between these samples that can explain the activity disparity.

3.2. XPS and TEM analysis

A great deal of analysis has been carried out on nitrogen-containing carbon, particularly with XPS, for coal and Li ion battery electrode applications. Analysis of the N 1s region with XPS can be used to differentiate between nitrogen species present in graphitic carbon, with quarternary-N and pyridinic-N being the most stable and abundant species in samples heated to 900°C [28]. Quarternary nitrogen is essentially nitrogen that has replaced carbon within the graphite layer, is bonded to three carbon atoms, and has a N 1s binding energy of 401.3 ± 0.3 eV. Pyridinic nitrogen has a N 1s binding energy of 398.6 ± 0.3 eV and is found on the edge of a graphite layer bonded to two carbon atoms, leaving a free electron pair sticking out from the graphite layer. Additionally, N 1s spectra of nitrogen containing graphite usually have a higher binding energy shoulder

(402–405 eV) that has been assigned to either quarternary-N or oxidized pyridinic-N [12, 28, 29].

In recent work, our group has noted that more active nitrogen-containing carbon ORR catalysts have more pyridinic nitrogen than less active samples [12]. Figure 2 shows the N 1s spectra of the HF washed samples, deconvoluted to fit the same species just mentioned. The more active samples have a higher pyridinic nitrogen content, as was observed for carbon grown samples. At this point, it is important to note that pyridinic-N is not being labeled as the active site for the ORR. Based on the data presented thus far and the work of others, however, it seems reasonable to say that the active site for the ORR is on the edge plane of the nitrogen-containing graphite [12, 16, 17, 30–32]. Therefore, the more active samples may contain more pyridinic nitrogen only because these samples have a higher proportion of edge planes exposed, and not necessarily because pyridinic-N itself is the source of activity. A useful method for verifying this hypothesis is high resolution TEM.

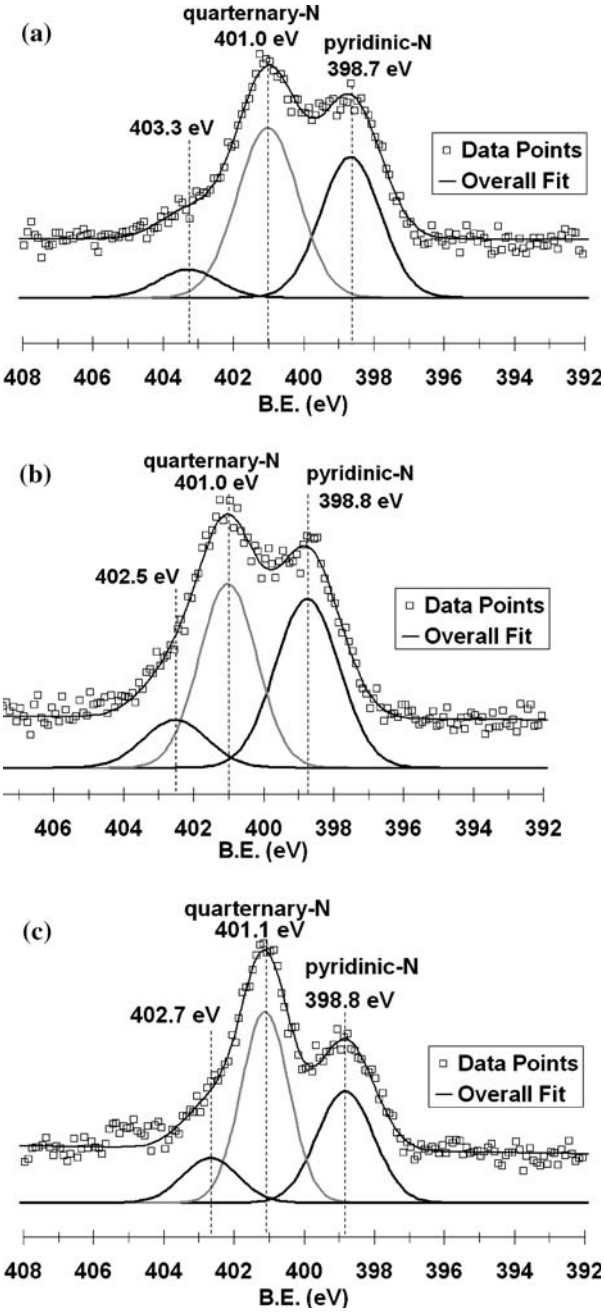

Figure 2. XPS analysis of the N 1s regions for samples treated 2 hours at 900°C with acetonitrile and subsequently washed with HF acid: (a) pure Al_2O_3, (b) 2% Fe/Al_2O_3, and (c) 2% Ni/Al_2O_3.

Microscopy images were obtained for the HF washed samples to relate the correlation between the trends seen in XPS and activity testing to the nano-structure of the carbon. The pure alumina-derived sample led to the formation of several types of nanostructures, shown in Figure 3. Surprisingly, fiber structures were found in the sample, as Figure 3a and d show. These fibers appear to have a ''compartmentalized'' or ''stacked cup'' structure, which is often reported for nitrogen-containing carbon fibers formed by various means [33]. These types of fibers would be expected to have more edge plane exposure than traditional multi-walled nanotubes, although not as high of edge exposure as ''stacked platelet'' carbon. Also present in the sample were structures representative of ''nano-onions'', shown in Figure 3b. These structures have virtually no edge plane exposure since they consist of concentric graphite spheres. A third type of structure observed was graphitic ribbons or sheets, shown in Figure 3c. The sample contained all three geometries without any of the structures being particularly dominant.

In contrast, the samples containing Fe or Ni nearly exclusively formed fiber structures during the acetonitrile decomposition. However, the structure of the fibers differed significantly depending on whether Fe or Ni was used. The lengths of the fibers were as much as several hundred microns, with the Ni grown fibers generally being longer than Fe grown fibers. The average diameter of the Fe derived fibers was 16 nm, while the fibers formed from Ni particles had an average diameter of 35 nm. Nevertheless, the most interesting difference between the fibers was the orientation of the graphite planes within the structures. Figure 4a shows a typical fiber in the Fe-derived sample. These fibers were mostly of the stacked cup structure, similar to the fibers formed in the pure alumina sample. The compartmentalized nature of these fibers and the fact that the tube walls are not parallel to the central fiber axis means that the fibers will have significant graphite edge exposure down the length of the structure. Conversely, a typical Ni-grown fiber is shown in Figure 4b. These fibers generally had thinner walls, with the planes oriented parallel to the central fiber axis, as is the case in conventional multi-walled nanotubes. Periodic graphite sheets oriented perpendicular to the central axis could be observed within the tube structure. These perpendicular sheets were spaced much further apart than the spacing of the

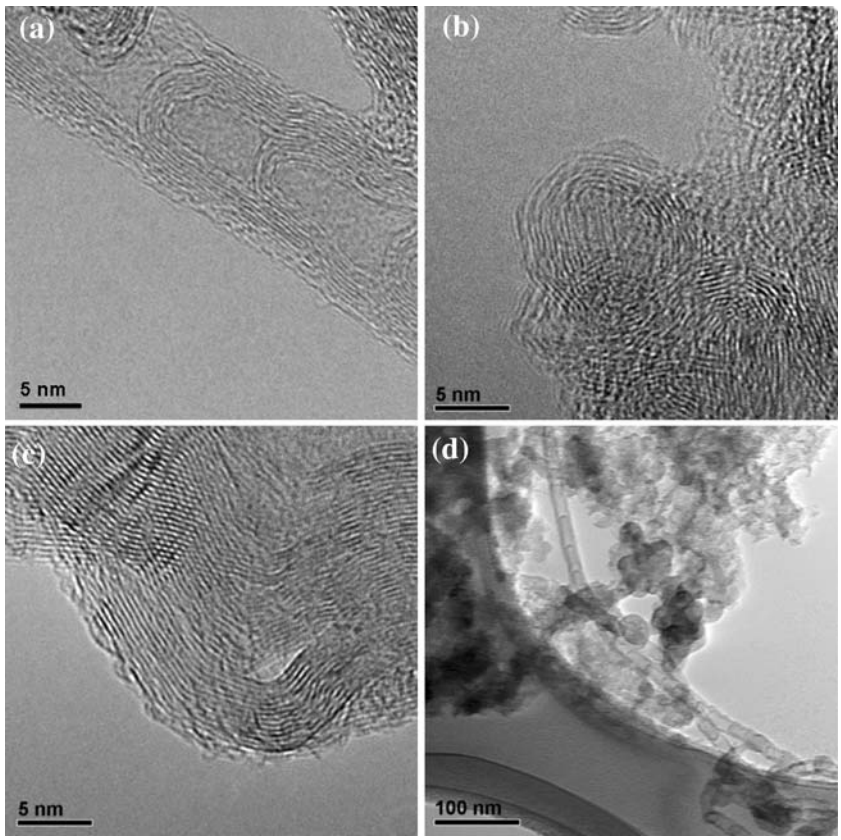

Figure 3. TEM images of HF acid washed nitrogen-containing carbon prepared from acetonitrile decomposition at 900°C over a pure alumina support; (a) fiber structure, (b) nano-onion structures, (c) graphitic ribbons or sheets, and (d) lower magnification depiction of a mixture of structures.

compartments in the Fe sample, and could possibly just belong to graphite sheets that peeled away from the inner tube walls.

Besides XPS analysis and activity testing, a bulk property observation that further supports the TEM images reported is hydrophobicity differences between the samples. Both the pure alumina formed and the Fe grown carbon samples could be dispersed in water by sonication. However, the Ni grown fibers could not be dispersed in water, and quickly fell out of suspension if sonicated or shaken vigorously in water. It is well-known that multi-walled nanotubes are super-hydrophobic. [34], which could explain these observed differences and would agree with the TEM imaging. Experiments to quantify the differences in hydrophobicity of these carbon structures will be presented in the next paper of this series.

At this point it is not exactly clear why different structures form from the different precursors. Crystal orientation, particle size, and metal-support interactions are all important parameters in fiber growth. Additionally, there are believed to be several possible mechanisms for fiber growth. In one mechanism carbon and nitrogen can adsorb onto a metal particle and diffuse into the particle forming a carbide/nitride intermediate. The carbon can then precipitate out of an opposing face of the particle, forming a graphite layer, with a concentration gradient being the driving force [19, 35, 36]. However, fibers can also form without the formation of a bulk carbide through surface diffusion of carbon species [19, 37]. Interestingly, Fe is thought to be able to form a nitride under similar conditions to this fiber growth, while Ni cannot [33]. Therefore, it is possible that the mechanism for nitrogen-containing carbon fiber formation is completely different for Ni and Fe particles, explaining the different structures observed. It is worth noting that fiber growth on pure alumina resulted in a similar structure to the fibers grown from Fe particles, and interestingly there was evidence of aluminum nitride formation in the alumina sample. However, a definitive mechanism cannot be proposed without further investigations.

3.3. Activity testing

Although the voltage of the oxygen reduction current peak reported in Tables 1 and 2 may be an effective way to compare the activities of samples, it does not necessarily correlate to how a catalyst will perform in an actual fuel cell. In addition to being catalytically active,

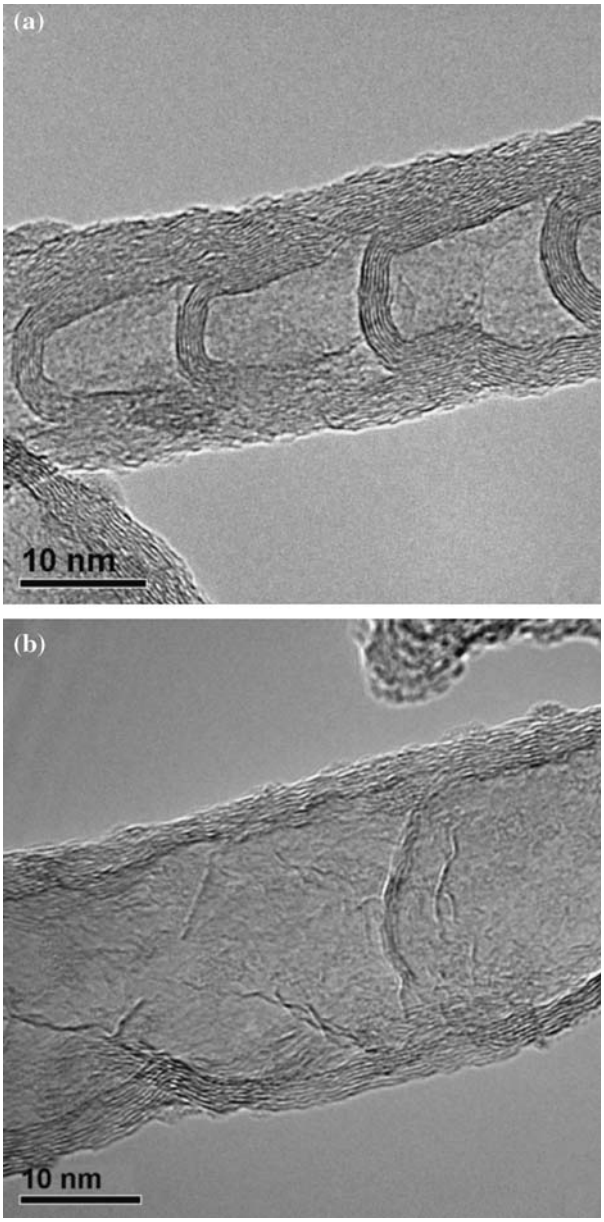

Figure 4. TEM images of HF washed nitrogen-containing carbon fiber structures formed from the decomposition of acetonitrile at 900°C over: (a) 2-wt% Fe / Al_2O_3, and (b) 2-wt% Ni / Al_2O_3.

cathode materials must be electrically conductive, proton conductive, and posses sufficient mass transfer properties to allow O_2 to diffuse into the electrode and water to diffuse out. To prevent corrosion of cell components and achieve better efficiency, ORR catalysts should also be highly selective to the formation of water, not hydrogen peroxide.

Rotating Ring-Disk Electrode (RDE) experiments can be used to measure selectivity of catalysts for the complete ORR, in addition to indicating relative ORR activity of samples [1]. Figure 5 shows disk currents during the initial sweep of CV's for the sample derived from acetonitrile pyrolysis over pure alumina and washed with HF acid. The background current taken in

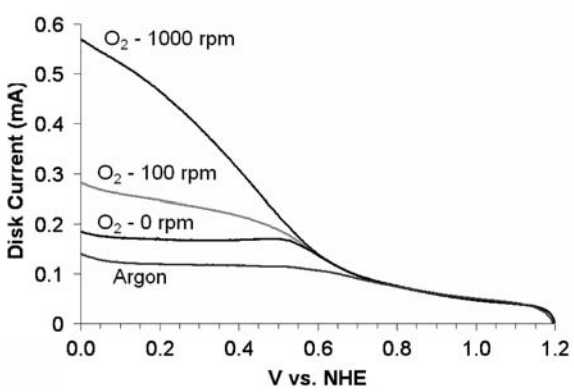

Figure 5. Disk currents during initial CV sweeps for the pure alumina sample treated 2 hours at 900°C with acetonitrile and subsequently washed with HF acid.

the argon sparged electrolyte originates from the double layer capacitance of the material as the voltage is swept. Once O_2 is added to the electrolyte, additional current arises from the ORR. Rotating the electrode increases the mass transfer of oxygen to the surface, thus increasing the reduction current at mass transfer limiting voltages. This figure is significant because these experiments demonstrate that oxygen is being reduced over a non-metal sample at relatively high potential. The voltage where the current peaks (indicating a transition from kinetic to mass transfer limited current) for this sample is approximately 540 mV vs. NHE. In the same set-up a 20 wt% Pt / Vulcan carbon catalyst peaks at 750 mV, while pure Vulcan Carbon XC-72 peaks at 30 mV.

The selectivity of the reaction can be monitored with the platinum ring of the RRDE. When held at a potential of 1.2 V vs. NHE, the ring cannot reduce O_2, but can reduce any H_2O_2 formed from the disk. Two possible reactions occurring on the disk during a CV are shown below:

$$O_2 + 4e^- + 4H^+ \rightarrow 2H_2O \quad (1.23V \text{ vs. NHE at STP})$$

$$O_2 + 2e^- + 2H^+ \rightarrow H_2O_2 \quad (1.76V \text{ vs. NHE at STP}).$$

The collection efficiency of the ring is known to be 20% when the RRDE is operating in a laminar flow regime, therefore, the ring current was only collected at 100 rpm of rotation in order to remain under laminar flow conditions. The results of these RRDE experiments are shown in Figure 6a–c. The ring current in these figures is multiplied by 5 to correct for the collection efficiency.

For the more conductive samples, the disk current undergoes a peak during the transition from kinetic limitations to mass transfer limitations. This is because the higher conductivity allows for a three dimensional active catalyst region in the thin catalyst film. Once mass transfer limits the reaction, then

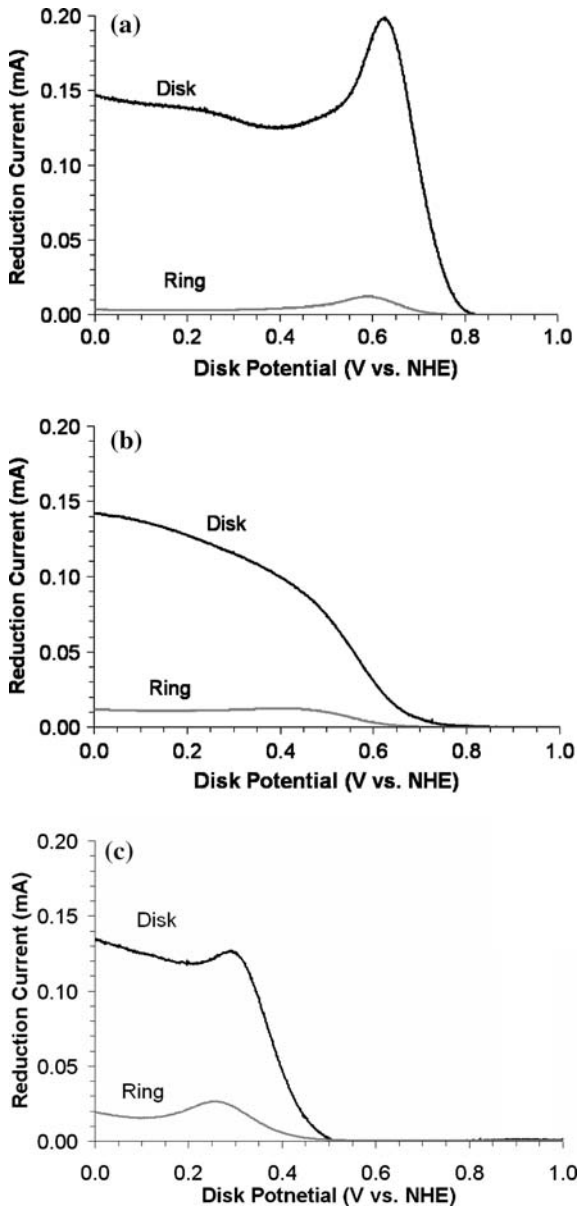

Figure 6. RRDE reduction currents for samples treated 2 hours at 900°C with acetonitrile and subsequently washed with HF acid: (a) 2% Fe / Al_2O_3, (b) pure $Al_2O_3$and (c) 2% Ni / Al_2O_3. The ring potential was held at 1.2 V and ring currents have been corrected for the collection efficiency.

the current is proportional to the two dimensional geometric area of the disk. Since the electrodes all have approximately the same geometric area, the currents eventually level out to the same value in the mass transfer limited region. However, the current also depends on the number of electrons being transferred in the reaction, so the currents are not identical. Such trends are discussed in more detail elsewhere [12,38].

The ring currents follow similar trends to the disk currents, although the relative intensities vary from sample to sample. The number of electrons being transferred per mole O_2 consumed can be determined from the equation:

$$n = 4[I_{disk}/(I_{disk} + (I_{ring}/N))],$$

where N = 0.20, the efficiency of the ring. For the more active Fe/Al_2O_3 derived sample, n is on average 3.91, indicating nearly complete conversion to water. For the Ni/Al_2O_3 derived sample, n is only 3.56, indicating significant peroxide formation, while the pure alumina sample has an average n of 3.70. Thus the correlation between activity and edge plane exposure also seems to hold for selectivity to water versus peroxide. Researchers have previously reported differences in the activity and selectivity of different carbon crystallographic planes for other reactions [31, 39], including the ORR in non-acidic electrolytes [16,17,30].

4. Conclusions

Nitrogen-containing carbon catalysts prepared by decomposition of acetonitrile over different supports were shown to be active for the oxygen reduction reaction to water in an acidic environment. Although catalysts prepared over supports that contained iron were more active, those prepared over alumina with no metal impurity also showed significant ORR activity, suggesting that a metal site is not needed for the oxygen reduction reaction. Instead, the metal particles may be acting as catalysts for the formation of active sites during the high temperature pyrolysis of the nitrogen and carbon containing precursor. One way that metal particles could catalyze the formation of active sites is through the growth of carbon nano-structures with a specific architecture.

The more active catalysts showed a higher exposure of graphite edge planes and a higher content of pyridinic nitrogen. The higher abundance of pyridinic nitrogen in these samples can be an end result of the specific carbon nano-structure that is formed, which exposes more of the edge planes. It is possible that Fe particles may be catalyzing the growth of carbon nano-structures with a higher percentage of the edge plane exposure, whether the precursor that is pyrolyzed is an organic macrocycle [16] or other C and N-containing species [12, 17]. At this point, it is not clear if nitrogen groups play a direct role in the oxygen reduction reaction by providing a site for the oxygen adsorption or their role is of a more indirect nature by simply increasing the electron donation ability of the carbon structure. It is also possible that pyridinic nitrogen itself may not have any involvement in the ORR, but rather be a marker for the edge plane exposure. In any case, it is clear that the active site for the ORR reaction does not require a metal center.

Although these carbon-based catalysts have substantial activity for the oxygen reduction reaction, further improvements may be necessary in other properties

of these materials, such as their conductivity and mass transfer characteristics, before they can be considered for PEM fuel cell applications. However, such improvements may be within reach considering the advancements being made in preparation of nanostructured carbon.

Acknowledgments

We gratefully acknowledge the financial support provided for this work by the National Science Foundation through Grants NSF-CTS-0437451, NSF-DGE-0221678, and NSF-DMR-0114098 and by the Ohio Department of Development through the Wright Center of Innovation Program.

References

[1] M. Lefevre and J.-P. Dodelet, Electrochimica Acta 48 (2003) 2749–2760.
[2] M. Lefevre, J.P. Dodelet and P. Bertrand, J. Phys. Chem. B 104 (2000) 11238.
[3] M. Lefevre, J.P. Dodelet and P. Bertrand, J. Phys. Chem. B. 106 (2002) 8705.
[4] S. Gupta, D. Tryk, I. Bae, W. Aldred and E. Yeager, J. Appl. Electrochem. 19 (1989) 19.
[5] G. Faubert, R. Cote, D. Guay, J.P. Dodelet, G. Denes, C. Poleunis and P. Bertrand, Electrochimica Acta 43 (1998) 1969.
[6] R. Cote, G. Lalande, D. Guay, J.P. Dodelet and G. Denes, J. Electrochem. Soc 145 (1998) 2411.
[7] H. Wang, R. Cote, G. Faubert, D. Guay, J. P. Dodelet, J. Phys. Chem. B 103 (1999).
[8] G. Lalande, R. Cote, D. Guay, J.P. Dodelet, L.T. Weng P. Bertrand, Electrochimi. Acta 42 (1997) 1379.
[9] G. Faubert, R. Côté, J.P. Dodelet, M. Lefèvre and P. Bertrand, Electrochimica Acta 44 (1999) 2589.
[10] F. Jaouen, S. Marcotte, J.-P. Dodelet and G. Lindbergh, J. Phys. Chem. B 107 (2003) 1376–1386.
[11] S. Ye and A.K. Vijh, Electrochem. Comm 5 (2003) 272–275.
[12] P.H. Matter, U.S. Ozkan and L. Zhang, J. Catal 239 (2006) 83–96.
[13] S. Gojkovic, S. Gupta and R. Savinell, J. Electroanaly. Chem. 462 (1999) 63–72.
[14] P. Gouerec, A. Biloul, O. Contamin, G. Scarbeck, M. Savy, J. Riga, L.T. Weng and P. Bertrand, J. Electroanal. Chem 422 (1997) 61.
[15] K. Wiesner, Electrochimica Acta 31 (1986) 1073–1078.
[16] S. Maldonado and K.J. Stevenson, J. Phys. Chem. B 108 (2004) 11375–11383.
[17] S. Maldonado and K.J. Stevenson, J. Phys. Chem. B 109 (2005) 4707–4716.
[18] G. Faubert, R. Cote, D. Guay, J.P. Dodlet, G. Denes and P. Bertrand, Electrochimica Acta 43 (1998) 341.
[19] R.T.K. Baker, Carbon 27 (1989) 315–323.
[20] N.M. Rodriguez, J. Mater. Res 8 (1993) 3233–3250.
[21] N.M. Rodriguez, A. Chambers and R.T.K. Baker, Langmuir 11 (1995) 3862–3866.
[22] C. Park and M.A. Keane, J. Catal 221 (2004) 386–399.
[23] A.-C. Dupuis, Prog. in Mater. Sci. 50 (2005) 929–961.
[24] R.T.K. Baker, M.S. Kim, A. Chambers, C. Park and N.M. Rodriguez, Stud. in Surf. Sci. and Catal. 111 (1997) 99–109.
[25] T. Nakajima and M. Koh, Carbon 35 (1997) 203.
[26] R. Kvon, G. Il'inich, A. Chuvilin and V. Likholobov, J. Mol. Catal. A: Chem. 158 (2000) 413.
[27] H.M. Liao, R.N.S. Sodhi and T.W. Coyle, J. Vac. Sci. Technol. A 11 (1993) 2681–2686.
[28] J.R. Pels, F. Kapteijn, J.A. Moulijn, Q. Zhu and K.M. Thomas, Carbon 33 (1995) 1641–1653.
[29] J. Casanovas, J.M. Ricart, J. Rubio, F. Illas and J.M. Jimenez-Mateos, J. Am. Chem. Soc 118 (1996) 8071–8076.
[30] K. Kinoshita, *Carbon, Electrochemical and Physiochemical Properties* (Wiley Interscience, New York, 1988).
[31] P. Chen, M.A. Fryling and R.L. McCreery, Analy. Chem. 67 (1995) 3115–3112.
[32] H.H. Yang and R.L. McCreery, J. Electrochem. Soc. 147 (2000) 3420.
[33] S. Trasobares, O. Stephan, C. Colliex, W.K. Hsu, H.W. Kroto and D.R.M. Walton, J. Chem. Phys. 116 (2002) 8966–8972.
[34] X.-L. Xie, Y.-W. Mai and X.-P. Zhou, Mat. Sci. Eng., R: Reports R49 (2005) 89–112.
[35] M. Audier and M. Coulon, Carbon 23 (1985) 317–323.
[36] A.J.H.M. Kock, P.K. de Boxx, E. Boellaard, W. Klop and J.W. Geus, J. Catal 96 (1985) 468–480.
[37] I. Alstrup, J. Catal 109 (1988) 241–251.
[38] A.J. Bard and L.R. Faulkner, *Electrochemical Methods: Fundamentals and Applications* (John Wiley and Sons Ltd, NY, 2001).
[39] K.K. Cline, M.T. McDermott and R.L. McCreery, J. Phys. Chem 98 (1994) 5314–5319.